

Scalar radiation emitted from a rotating source around a Reissner-Nordström black hole

Luís C. B. Crispino*

Faculdade de Física, Universidade Federal do Pará, 66075-110, Belém, PA, Brazil

André R. R. da Silva† and George E. A. Matsas‡

Instituto de Física Teórica, Universidade Estadual Paulista, Rua Pamplona 145, 01405-900, São Paulo, SP, Brazil

(Received 4 June 2008; published 7 January 2009)

We investigate the radiation emitted from a scalar source in circular orbit around a Reissner-Nordström black hole. Particle and energy emission rates are analytically calculated in the *low*- and *high*-frequency regimes and shown to be in full agreement with a numerical calculation. A brief comment connecting the present work with a recent discussion on the cosmic censorship conjecture is included at the end.

DOI: 10.1103/PhysRevD.79.024004

PACS numbers: 04.62.+v, 04.20.Dw, 41.60.-m

I. INTRODUCTION

The mounting evidences favoring the existence of black holes and the perception that they are usually surrounded by accretion disks has raised much interest in the study of the radiation emitted from their vicinities. In this context Misner and collaborators [1,2] initiated the so-called *gravitational synchrotron radiation* program in the 1970's, where classical radiation emitted from charges in motion around black holes was analyzed. This was followed up by a number of related investigations in different situations of interest up to these days using classical and quantum approaches (see, e.g., Ref. [3] and references therein).

In this paper we analyze the scalar radiation of Klein-Gordon particles emitted from sources in geodesic orbit around Reissner-Nordström black holes. We work in the context of standard QFTCS (see Refs. [4,5] for comprehensive accounts). As far as the emitted particles have small angular momentum and energy in comparison to the black hole mass, no significant backreaction effects are expected and, thus, the background spacetime can be regarded as fixed. Because of the difficulty to express the solution of some differential equations, which we deal with in terms of known special functions, our computations are performed (i) numerically but without further approximations and (ii) analytically but restricted to the low- and high-frequency regimes. The paper is organized as follows: In Sec. II, we present the general formulas for the emission rate and radiated power of scalar particles from the monopole source in circular orbit around the Reissner-Nordström black hole. In Sec. III, we present analytic results in the low- and high-energy regimes. In Sec. IV, the analytic results obtained in the previous section are plotted against a full numerical calculation and shown to agree. We also compute the amount of the emitted radiation, which reaches asymptotic observers rather than being

absorbed by the hole and the angular distribution of the emitted radiation with respect to the orbit plane. In Sec. V, we establish a connection between the particles generated by the present mechanism and the ones considered in Refs. [6,7], where the validity of the cosmic censorship conjecture was discussed. Section VI is dedicated to our final remarks. We assume natural units $c = G = \hbar = 1$ unless stated otherwise.

II. EMISSION RATES AND RADIATED POWERS

The line element of a Reissner-Nordström black hole with mass M and electric charge $|Q| \leq M$ can be written as [8]

$$ds^2 = f(r)dt^2 - f(r)^{-1}dr^2 - r^2(d\theta^2 + \sin^2\theta d\varphi^2), \quad (2.1)$$

where

$$f(r) \equiv (1 - r_+/r)(1 - r_-/r) \quad (2.2)$$

and $r_{\pm} \equiv M \pm \sqrt{M^2 - Q^2}$. Outside the outer event horizon, i.e., for $r > r_+$, we have a global timelike isometry generated by the Killing field ∂_t .

Now we introduce a free massless scalar field $\Phi = \Phi(x^\mu)$ satisfying $\square\Phi = 0$. The corresponding field operator can be expanded in terms of creation $a_{\omega l m}^{\alpha\dagger}$ and annihilation $a_{\omega l m}^{\alpha}$ operators as

$$\hat{\Phi}(x^\mu) = \sum_{\alpha=\leftarrow}^{\rightarrow} \sum_{l=0}^{\infty} \sum_{m=-l}^l \int_0^{\infty} d\omega [u_{\omega l m}^{\alpha}(x^\mu) a_{\omega l m}^{\alpha} + \text{H.c.}], \quad (2.3)$$

where the normal modes are written as

$$u_{\omega l m}^{\alpha} = \sqrt{\frac{\omega}{\pi}} \frac{\psi_{\omega l}^{\alpha}(r)}{r} Y_{lm}(\theta, \varphi) e^{-i\omega t} \quad (2.4)$$

and are assumed to be orthonormalized according to the Klein-Gordon inner product [4]. Here, $\omega \geq 0$ and $l \geq 0$, $m \in [-l, l]$ are frequency and angular momentum quantum numbers, respectively, and $\alpha = \leftarrow (\rightarrow)$ labels ingoing

*crispino@ufpa.br

†dasilva@ift.unesp.br

‡matsas@ift.unesp.br

(outgoing) modes. $Y_{lm}(\theta, \varphi)$ are the usual spherical harmonics. $\psi_{\omega l}^{\leftarrow}(r)$ and $\psi_{\omega l}^{\rightarrow}(r)$ are associated with purely incoming modes from the past null infinity \mathcal{I}^- and outgoing from the past white-hole horizon \mathcal{H}^- , respectively. $\psi_{\omega l}^{\alpha}$ satisfies

$$\left[-f(r) \frac{d}{dr} \left(f(r) \frac{d}{dr} \right) + V_{\text{eff}}(r) \right] \psi_{\omega l}^{\alpha}(r) = \omega^2 \psi_{\omega l}^{\alpha}(r), \quad (2.5)$$

where

$$V_{\text{eff}}(r) = \left(1 - \frac{2M}{r} + \frac{Q^2}{r^2} \right) \left(\frac{2M}{r^3} - \frac{2Q^2}{r^4} + \frac{l(l+1)}{r^2} \right) \quad (2.6)$$

is the effective scattering potential (see, e.g., Ref. [9] for more detail). A plot of the scattering potential can be found in Fig. 1. The larger the l the larger the V_{eff} because of the centrifugal barrier. By performing the coordinate transformation

$$x \equiv y + \frac{(y_+)^2 \ln|y - y_+| - (y_-)^2 \ln|y - y_-|}{y_+ - y_-}, \quad (2.7)$$

where $y \equiv r/2M$ and $y_{\pm} \equiv r_{\pm}/2M$, Eq. (2.5) can be cast in the form

$$(-d^2/dx^2 + 4M^2 V_{\text{eff}}[r(x)]) \psi_{\omega l}^{\alpha}(x) = 4M^2 \omega^2 \psi_{\omega l}^{\alpha}(x). \quad (2.8)$$

$$\psi_{\omega l}^{\leftarrow}(x) \approx \frac{1}{2\omega} \begin{cases} \mathcal{T}_{\omega l}^{\leftarrow} e^{-2iM\omega x} & (x < 0, |x| \gg 1) \\ 2(-i)^{l+1} M\omega x h_l^{(1)}(2M\omega x)^* + 2i^{l+1} \mathcal{R}_{\omega l}^{\leftarrow} M\omega x h_l^{(1)}(2M\omega x) & (x \gg 1) \end{cases} \quad (2.10)$$

and

$$\psi_{\omega l}^{\rightarrow}(x) \approx \frac{1}{2\omega} \begin{cases} e^{2iM\omega x} + \mathcal{R}_{\omega l}^{\rightarrow} e^{-2iM\omega x} & (x < 0, |x| \gg 1) \\ 2i^{l+1} \mathcal{T}_{\omega l}^{\rightarrow} M\omega x h_l^{(1)}(2M\omega x) & (x \gg 1) \end{cases}. \quad (2.11)$$

Here, $|\mathcal{R}_{\omega l}^{\alpha}|^2$ and $|\mathcal{T}_{\omega l}^{\alpha}|^2$ are the reflection and transmission coefficients, respectively, satisfying the usual probability conservation equation: $|\mathcal{R}_{\omega l}^{\alpha}|^2 + |\mathcal{T}_{\omega l}^{\alpha}|^2 = 1$ and $h_l^{(1)}(2M\omega x)$ is the spherical Hankel function. Note that $h_l^{(1)}(x) \approx (-i)^{l+1} \exp(ix)/x$ for $|x| \gg 1$.

Now, let us consider a monopole

$$j(x^\nu) = \frac{q}{\sqrt{-g}u^0} \delta(r - R_S) \delta(\theta - \pi/2) \delta(\varphi - \Omega t) \quad (2.12)$$

describing a scalar source in uniform circular motion at the equatorial plane of the Reissner-Nordström black hole, i.e., $\theta = \pi/2$, with $r = R_S$ and angular velocity $\Omega \equiv d\phi/dt = \text{const} > 0$ as defined by asymptotic static observers. Here, $g \equiv \det(g_{\mu\nu})$ and

$$u^\mu(\Omega, R_S) = (f(R_S) - R_S^2 \Omega^2)^{-1/2} (1, 0, 0, \Omega) \quad (2.13)$$

is the four velocity of the source. By assuming that the source is free of interactions other than the gravitational

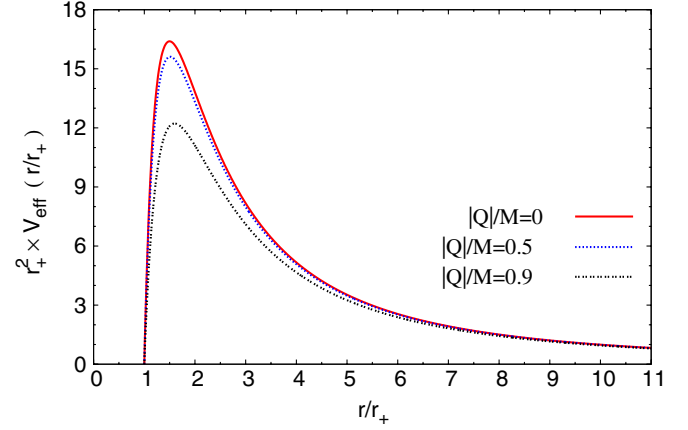


FIG. 1 (color online). The effective scattering potential for $|Q|/M = 0, 0.5$ and 0.9 is plotted for $l = 10$ as a function of r/r_+ . The larger the $|Q|/M$ the smaller the $V_{\text{eff}}(r/r_+)$.

Accordingly, the creation and annihilation operators satisfy the simple commutation relations

$$[a_{\omega l m}^{\alpha}, a_{\omega' l' m'}^{\alpha' \dagger}] = \delta_{\alpha\alpha'} \delta_{ll'} \delta_{mm'} \delta(\omega - \omega'), \quad (2.9)$$

where the state $|0\rangle$, defined by $a_{\omega l m}^{\alpha} |0\rangle = 0$ for every α, ω, l , and m , is denominated *Boulware vacuum*. Close ($x < 0, |x| \gg 1$) to and far away ($x \gg 1$) from the horizon we have

one, we obtain that

$$\Omega = \sqrt{M/R_S^3 - Q^2/R_S^4}, \quad (2.14)$$

where

$$R_S > r_{\text{ph}} = (3M + \sqrt{9M^2 - 8Q^2})/2. \quad (2.15)$$

Here, r_{ph} is the radius of the null circular geodesic and defines the innermost limit to timelike geodesic circular orbits. We note, moreover, that we have normalized the source $j(x^\mu)$ in Eq. (2.12) by requiring that $\int d\sigma j(x^\mu) = q = \text{const}$, where $d\sigma$ is the proper three-volume element orthogonal to u^μ .

Next, let us minimally couple the source to the field through the interaction action

$$\hat{S}_I = \int d^4x \sqrt{-g} j \hat{\Phi}. \quad (2.16)$$

From this we can interpret q in Eq. (2.12) as a coupling constant between source and field. Then the emission amplitude at the tree level of one scalar particle with quantum numbers (α, ω, l, m) into the Boulware vacuum is given by

$$\mathcal{A}_{\alpha\omega lm}^{\text{em}} = \langle \alpha\omega lm | i\hat{S}_l | 0 \rangle = i \int d^4x \sqrt{-g} j(x^\mu) u_{\omega lm}^{\alpha*}. \quad (2.17)$$

Note that for sources in constant circular motion the amplitude $\mathcal{A}_{\alpha\omega lm}^{\text{em}}$ is proportional to $\delta(\omega - \omega_0)$, where we have defined $\omega_0 \equiv m\Omega$. Hence, the frequency of the emitted particles is constrained by the relation $\omega = \omega_0$. In particular, since $\Omega > 0$, no waves with $m \leq 0$ are emitted. The emission rate $\Gamma_{\alpha\omega_0 l}$ and corresponding emitted power $W_{\alpha\omega_0 l}$ of particles with quantum numbers (α, ω_0, l) ($l \geq 1$) are given by

$$\begin{aligned} \Gamma_{\alpha\omega_0 l} &= \int_0^{+\infty} d\omega |\mathcal{A}_{\alpha\omega lm}^{\text{em}}|^2 / T \\ &= 2q^2 \omega_0 (f(R_S) - R_S^2 \Omega^2) |\psi_{\omega_0 l}^\alpha(R_S) / R_S|^2 \\ &\quad \times |Y_{lm}(\pi/2, 0)|^2 \end{aligned} \quad (2.18)$$

and

$$\begin{aligned} W_{\alpha\omega_0 l} &= \int_0^{+\infty} d\omega \omega |\mathcal{A}_{\alpha\omega lm}^{\text{em}}|^2 / T \\ &= 2q^2 \omega_0^2 (f(R_S) - R_S^2 \Omega^2) |\psi_{\omega_0 l}^\alpha(R_S) / R_S|^2 \\ &\quad \times |Y_{lm}(\pi/2, 0)|^2, \end{aligned} \quad (2.19)$$

respectively, where $T = 2\pi\delta(0)$ is the total time as measured by asymptotic observers [10]. Note also that $Y_{lm}(\pi/2, 0) = 0$ if $l + m$ is odd and

$$|Y_{lm}(\pi/2, 0)|^2 = \frac{2l+1}{4\pi} \frac{(l+m-1)!!(l-m-1)!!}{(l+m)!!(l-m)!!} \quad (2.20)$$

if $l + m$ is even [11]. We have defined $n!! \equiv n(n-2)\cdots 1$ if n is odd, $n!! \equiv n(n-2)\cdots 2$ if n is even, and $(-1)!! \equiv 1$. Moreover, note that if we had chosen the Unruh or Hartle-Hawking vacua rather than the Boulware one, then Eqs. (2.18) and (2.19) would be associated with the *net* emitted radiation since the absorption and stimulated emission rates (which are induced by the presence of thermal fluxes) are the same.

The total emission rate Γ^{total} and radiated power W^{total} are obtained by summing on the quantum numbers α, l, m in Eqs. (2.18) and (2.19), accordingly. The total particle and energy rates which escape to infinity are

$$\Gamma^{\text{obs}} = \sum_{l=1}^{\infty} \sum_{m=1}^l (|\mathcal{T}_{\omega_0 l}^{\rightarrow}|^2 \Gamma_{\rightarrow\omega_0 l} + |\mathcal{R}_{\omega_0 l}^{\leftarrow}|^2 \Gamma_{\leftarrow\omega_0 l}) \quad (2.21)$$

and

$$W^{\text{obs}} = \sum_{l=1}^{\infty} \sum_{m=1}^l (|\mathcal{T}_{\omega_0 l}^{\rightarrow}|^2 W_{\rightarrow\omega_0 l} + |\mathcal{R}_{\omega_0 l}^{\leftarrow}|^2 W_{\leftarrow\omega_0 l}), \quad (2.22)$$

respectively. Here, we note that $\mathcal{T}_{\omega_0 l}^{\leftarrow} = \mathcal{T}_{\omega_0 l}^{\rightarrow}$. This guarantees that $|\mathcal{R}_{\omega_0 l}^{\leftarrow}| = |\mathcal{R}_{\omega_0 l}^{\rightarrow}|$. Note, however, that $\mathcal{R}_{\omega_0 l}^{\leftarrow}$ and

$\mathcal{R}_{\omega_0 l}^{\rightarrow}$ will in general differ by a phase (in contrast to $\mathcal{T}_{\omega_0 l}^{\leftarrow}$ and $\mathcal{T}_{\omega_0 l}^{\rightarrow}$).

The power angular distribution per unit of solid angle, Ω_s , at fixed frequency ω_0 is well estimated by [2]

$$\frac{dW_{\omega_0 l}(\theta, \phi)}{d\Omega_s} = \sum_{\alpha=\leftarrow}^{\rightarrow} W_{\alpha\omega_0 l} |Y_{ll}(\theta, \phi)|^2 \quad (2.23)$$

for $\omega_0 = m\Omega$ ($m = l$) and

$$|Y_{ll}(\theta, \phi)|^2 = \frac{(2l+1)[(2l-1)!!]^2}{4\pi(2l)!} \sin^{2l}\theta.$$

III. LOW- AND HIGH-ENERGY SOLUTIONS

Now, in order to calculate the physical observables given by Eqs. (2.18), (2.19), (2.21), and (2.22), we must work out the functions $\psi_{\omega l}^\alpha(r)$. We exhibit approximate low- and high-frequency solutions, which are going to be used in the next section in conjunction with a full numerical calculation designed to cover the whole frequency range.

A. Low-energy solutions

The low-frequency solution for $\psi_{\omega l}^\alpha(r)$ has been already worked out in Ref. [9] and can be cast (up to an arbitrary phase) in the form

$$\psi_{\omega l}^{\rightarrow}(r) = \frac{-4iM y_+ y_- Q_l[z(y)]}{y_+ - y_-} \quad (3.1)$$

and

$$\psi_{\omega l}^{\leftarrow}(r) = \frac{2^{2l+1} (-i)^{l+1} (l!)^3 M^{l+1} (y_+ - y_-)^l \omega^l y P_l[z(y)]}{(2l+1)!(2l)!}, \quad (3.2)$$

where

$$z(y) \equiv \frac{2y-1}{y_+ - y_-}. \quad (3.3)$$

One can also obtain

$$\mathcal{T}_{\omega l}^{\rightarrow} = \frac{2^{2l+2} (-i)^{l+1} y_+ (y_+ - y_-)^l (l!)^3 (M\omega)^{l+1}}{(2l+1)!(2l)!} \quad (3.4)$$

in the low-frequency regime. We recall that $\mathcal{T}_{\omega l}^{\leftarrow} = \mathcal{T}_{\omega l}^{\rightarrow}$. Equation (3.4) was used in Ref. [6] to calculate the probability $|\mathcal{T}_{\omega l}^{\rightarrow}|^2$ of a wave to tunnel into the black hole assuming a fixed Reissner-Nordström effective scattering potential. The larger the black hole mass and charge in comparison with the wave energy and angular momentum the better the static potential approximation. Here, we consider large enough black holes in order to neglect spacetime backreaction effects.

B. High-energy solutions

A good approximation of $\psi_{\omega l}^\alpha(r)$ for high energies can be obtained by using the WKB approximation (see, e.g., Ref. [12]). To do so, it is worth noting that Eq. (2.8) resembles the one-dimensional Schrödinger equation. By considering the effective energy ω^2 lower than the peak of

$$\psi_{\omega l}^\leftarrow(x) \approx \frac{A_\omega^\leftarrow}{\sqrt{k_{\omega l}}} \begin{cases} \mathcal{T}_{\omega l}^\leftarrow e^{-i(\sigma_{\omega l} - \pi/4)} & (x < 0, |x| \gg 1) \\ e^{-i(\rho_{\omega l} + \pi/4)} + \mathcal{R}_{\omega l}^\leftarrow e^{i(\rho_{\omega l} + \pi/4)} & (x \gg 1) \end{cases} \quad (3.5)$$

and

$$\psi_{\omega l}^\rightarrow(x) \approx \frac{A_\omega^\rightarrow}{\sqrt{k_{\omega l}}} \begin{cases} \mathcal{R}_{\omega l}^\rightarrow e^{-i(\sigma_{\omega l} - \pi/4)} + e^{i(\sigma_{\omega l} - \pi/4)} & (x < 0, |x| \gg 1) \\ \mathcal{T}_{\omega l}^\rightarrow e^{i(\rho_{\omega l} + \pi/4)} & (x \gg 1) \end{cases}, \quad (3.6)$$

where we have defined

$$\sigma_{\omega l}(x) \equiv \int_{x_-}^x k_{\omega l}(x') dx'$$

and

$$\rho_{\omega l}(x) \equiv \int_{x_+}^x k_{\omega l}(x') dx'$$

with $k_{\omega l}(x) \equiv 2M\sqrt{\omega^2 - V_{\text{eff}}(x)}$. Here, the normalization constants A_ω^α are determined by an asymptotic fitting between Eqs. (2.10), (2.11), (3.5), and (3.6), respectively. As a result, we obtain $|A_\omega^\leftarrow| = |A_\omega^\rightarrow| = \sqrt{M/2\omega}$.

Now, we must analyze the case $V_{\text{eff}}(x) > \omega^2$, which occurs in the interval (x_-, x_+) . In this region, $\psi_{\omega l}^\alpha(r)$ can be cast in the form

$$\psi_{\omega l}^\leftarrow(x) \approx -i \frac{A_\omega^\leftarrow}{\sqrt{\kappa_{\omega l}}} e^{-\xi_{\omega l}} \quad (3.7)$$

and

$$\psi_{\omega l}^\rightarrow(x) \approx -i \frac{A_\omega^\rightarrow}{\sqrt{\kappa_{\omega l}}} e^{(\Theta_{\omega l} + \xi_{\omega l})} \quad (3.8)$$

assuming $\kappa_{\omega l}^{-1} d(\ln \kappa_{\omega l})/dx \ll 1$, where we have defined

$$\xi_{\omega l}(x) \equiv \int_x^{x_+} \kappa_{\omega l}(x') dx'$$

and

$$\Theta_{\omega l} \equiv - \int_{x_-}^{x_+} \kappa_{\omega l}(x) dx$$

with $\kappa_{\omega l}(x) \equiv 2M\sqrt{V_{\text{eff}}(x) - \omega^2}$. The quantity $\Theta_{\omega l}$ is the well-known barrier factor and is associated with the transmission coefficient by

$$|\mathcal{T}_{\omega l}^\alpha|^2 \approx e^{2\Theta_{\omega l}}. \quad (3.9)$$

As a consequence, $|\mathcal{R}_{\omega l}^\alpha|^2 \approx 1 - e^{2\Theta_{\omega l}}$.

C. Numerical calculation

Now, in order to plot particle and energy emission rates in the whole frequency range, a numerical calculation

$V_{\text{eff}}(x)$, one has two distinct situations. The first one is characterized by $V_{\text{eff}}(x) < \omega^2$, which is valid in the intervals $(-\infty, x_-)$ and $(x_+, +\infty)$, where x_\pm ($x_- < x_+$) stands for the classical turning points, which satisfy $V_{\text{eff}}(x_\pm) = \omega^2$. Then, in the region where $k_{\omega l}^{-1} d(\ln k_{\omega l})/dx \ll 1$ is satisfied, we write down

procedure is in order. Briefly speaking the numerical method consists of solving Eq. (2.8) for the left- and right-moving radial functions $\psi_{\omega l}^\leftarrow(r)$ and $\psi_{\omega l}^\rightarrow(r)$ with asymptotic boundary conditions compatible with Eqs. (2.10) and (2.11), respectively. We refer to Ref. [13] for more detail.

IV. RESULTS

In Figs. 2 and 3 we show the particle emission rates for $l = m = 5$, and $\alpha = \leftarrow$ and \rightarrow , respectively. We also display a zoom for $M\Omega \ll 1$. We can see the good approximation provided by our low-energy formulas, which are applicable when the source is in circular orbits far away from the horizon. In the same token, the results obtained

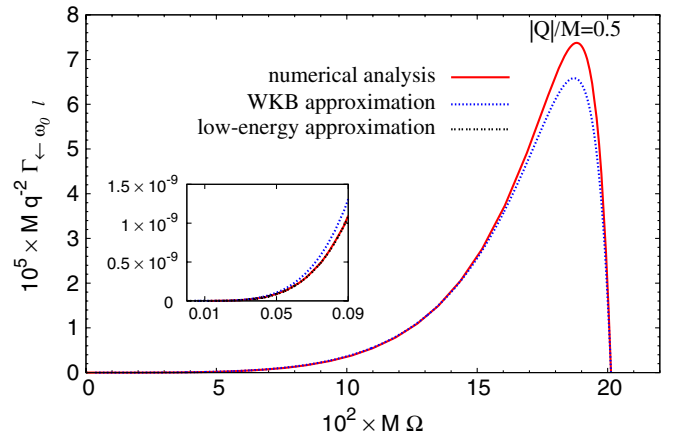


FIG. 2 (color online). The numerical result for $\Gamma_{\leftarrow\omega_0 l}$ with $l = m = 5$ is shown assuming a black hole with $|Q|/M = 0.5$. The internal box is a zoom of the $\Omega M \ll 1$ region and shows the excellent agreement obtained with our low-energy formulas. The numerical and low-energy results are superimposed and cannot be distinguished with the present resolution. We also plot in this region the result obtained with the WKB method to make it clear that it captures the qualitative behavior in the low-energy region as well. Finally, we emphasize the very nice quantitative approximation provided by the WKB method in the $R_S \approx r_{\text{ph}}$ region ($\Omega M \approx 0.2$).

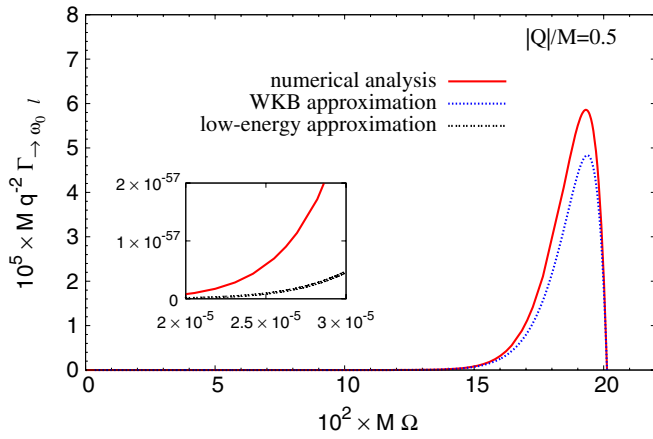


FIG. 3 (color online). The numerical result for $\Gamma_{\rightarrow\omega_0 l}$ with $l = m = 5$ and $|Q|/M = 0.5$ is plotted. We can see the convergence of the numerical calculation with (i) low-energy analytical results for $\Omega M \ll 1$ and (ii) the WKB method for $R_S \approx r_{\text{ph}}$ ($\Omega M \approx 0.2$).

using the WKB approximation reproduce very well the curves for $R_S \approx r_{\text{ph}}$, i.e., when the source is close to the innermost timelike geodesic circular orbit. This is the region where most emitted particles are high-energy ones. This is also convenient to notice that the WKB approximation reproduces most qualitative aspects of the exact numerical calculation. The WKB approximation is specially good for large angular momentum quantum numbers l , as expected. This is very handy when dealing with

large l solutions, since the WKB method requires comparatively modest computational resources in contrast to the full numerical procedure. In Figs. 4 and 5, we analyze in more detail the low- and high-energy particle emission regions by using the proper formulas, namely, Eq. (2.18) with Eqs. (3.1), (3.2), (3.7), and (3.8), respectively. We note that $\Gamma_{\leftarrow\omega_0 l}$ is typically larger than $\Gamma_{\rightarrow\omega_0 l}$ except for $R_S \approx r_{\text{ph}}$ and that the larger the l the smaller the $\Gamma_{\alpha\omega_0 l}$. (For a fixed l the larger the m the larger the contribution provided that $l + m$ is even.) Moreover, the presence of charge in the black hole tends to damp $\Gamma_{\alpha\omega_0 l}$. In Figs. 6 and 7, we analyze in more detail the radiated power in the regions, where the source is far away from the horizon and close to the innermost timelike geodesic orbit by using Eq. (2.19) with Eqs. (3.1), (3.2), (3.7), and (3.8), respectively. Far away from the hole the leading contribution to the power comes from the mode with $l = m = 1$, while for $R_S \approx r_{\text{ph}}$ this will depend on the source angular velocity Ω . In Figs. 8 and 9, we plot the particle emission rate and corresponding power, which reach asymptotic observers for $|Q|/M = 0.5$, respectively. It is worth noting that for $R_S \approx r_{\text{ph}}$ about half of the emitted particles are absorbed by the hole. The WKB and the low-energy approximations are in nice agreement with the numerical results. In Fig. 10, we plot the total power emitted as a function of the angular momentum quantum number l for fixed Ω : $W_\lambda^{\text{total}} \equiv \sum_{m=1}^l W_{\lambda\omega_0 l}$. Note that large l 's are excited for $R_S \approx r_{\text{ph}}$. Besides, both modes $\lambda = \leftarrow$ and \rightarrow contribute approximately the same (in agreement with the analysis above).

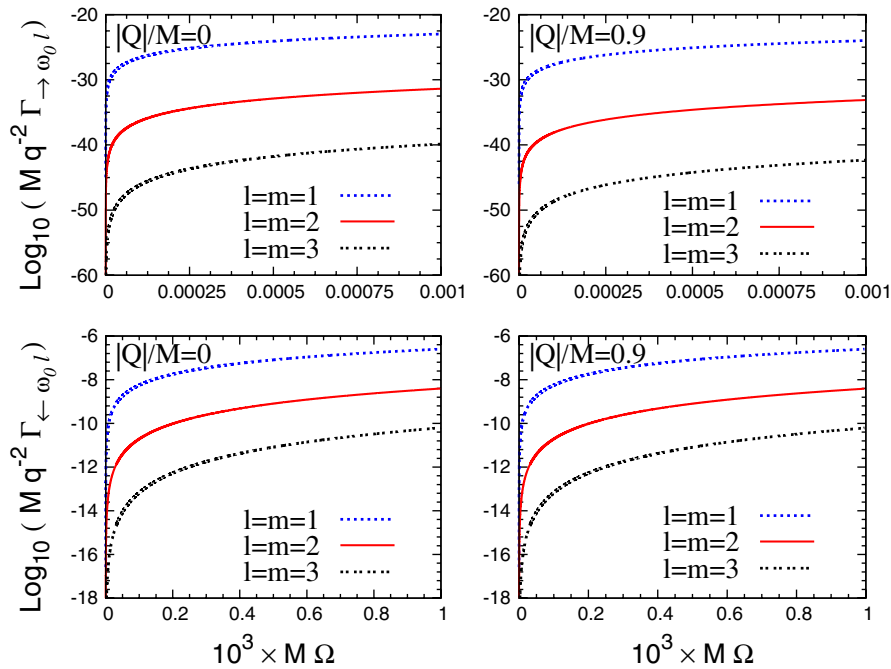


FIG. 4 (color online). The particle emission rates $\Gamma_{\alpha\omega_0 l}$ ($\alpha = \leftarrow, \rightarrow$) are plotted in the low-frequency regime as a function of the source angular velocity Ω for different values of l ($m = l$). $\Gamma_{\leftarrow\omega_0 l}$ is seen to be larger than $\Gamma_{\rightarrow\omega_0 l}$. The larger the l and $|Q|/M$ the smaller the $\Gamma_{\alpha\omega_0 l}$.

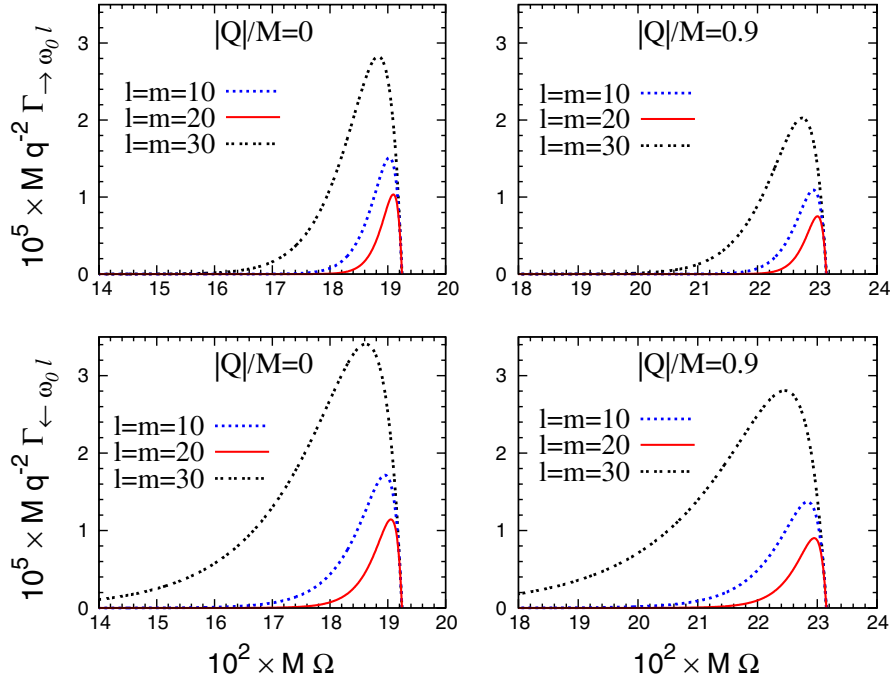


FIG. 5 (color online). The particle emission rates $\Gamma_{\alpha\omega_0 l}$ are plotted in the high-frequency regime for different values of l ($m = l$). The qualitative behavior of $\Gamma_{\alpha\omega_0 l}$ are much like the ones observed in the low-frequency regime with one exception, namely, $\Gamma_{-\omega_0 l}$ becomes larger than $\Gamma_{+\omega_0 l}$ for $R_S \approx r_{\text{ph}}$. The existence of charge in the black hole makes $\Gamma_{\alpha\omega_0 l}$ to decrease. The figures are plotted up to the last timelike geodesic circular orbit.

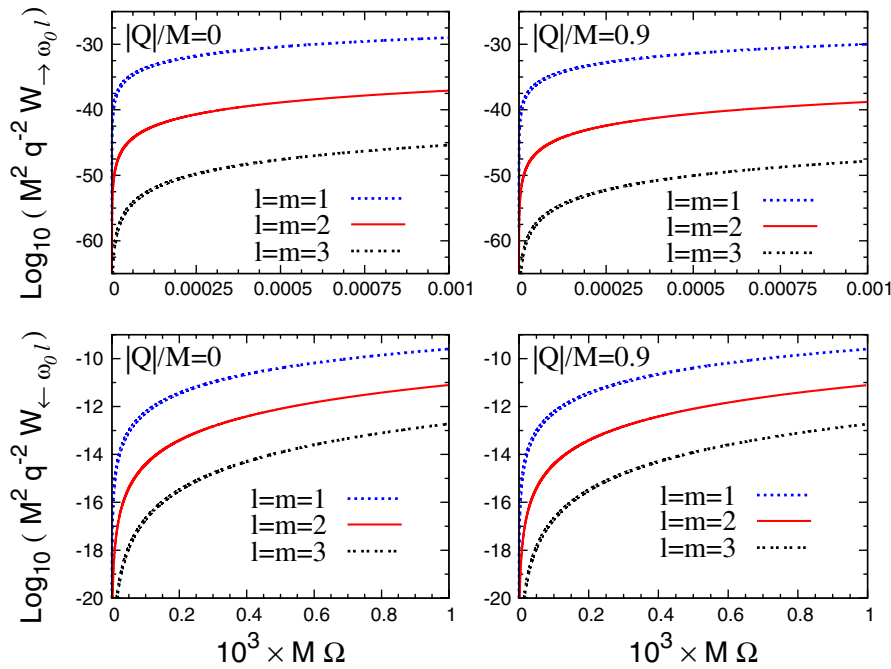


FIG. 6 (color online). The radiated powers $W_{\alpha\omega_0 l}$ ($\alpha = \leftarrow, \rightarrow$) are plotted in the low-frequency regime as a function of the source angular velocity Ω for different values of l ($m = l$). The qualitative behavior of $W_{\alpha\omega_0 l}$ and $\Gamma_{\alpha\omega_0 l}$ are similar to each other in the low-frequency regime in contrast to what we see in the high-frequency one.

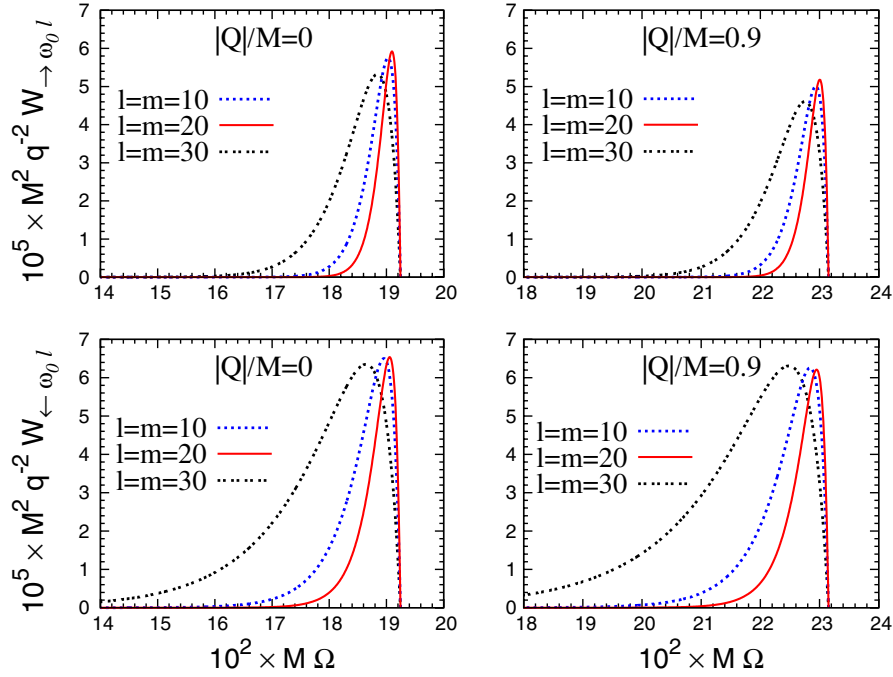


FIG. 7 (color online). The radiated powers $W_{\alpha\omega_0 l}$ ($\alpha \leftarrow, \rightarrow$) are plotted in the high-frequency regime. Note that depending on the value of Ω different l values contribute the most.

Finally, in Figs. 11 and 12 we examine the power angular distribution per unit of solid angle (2.23) with respect to the orbital plane when the source is far away and close to the most internal circular geodesic, respectively. We see that most radiated power is beamed into a narrow angle interval around the orbital plane when $R_S \approx r_{\text{ph}}$, which is a typical feature of the synchrotron radiation.

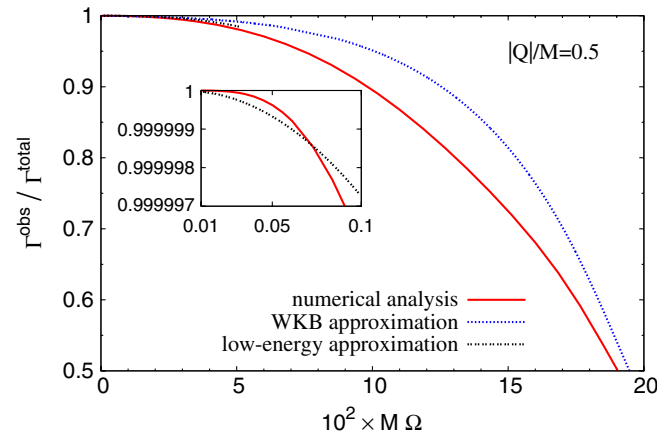


FIG. 8 (color online). We plot the rate of particles, which reach asymptotic observers as a function of Ω for $|Q|/M = 0.5$. The sum in Eq. (2.21) is taken up to $l = 5$. It is seen that the WKB and the low-energy approximation give good results in the proper regions, as expected. It is interesting to note that for $R_S \approx r_{\text{ph}}$ ($\Omega M \approx 0.2$) about half of the emitted particles are lost inside the hole.

V. CONNECTION WITH THE COSMIC CENSORSHIP CONJECTURE

Recently, [6,7] it was investigated whether or not a scalar particle with *small energy* but *large enough angular momentum* could tunnel through the gravitational scattering potential of a nearly extreme macroscopic Reissner-Nordström black hole $|Q|/M \leq 1$, whereby it would acquire enough angular momentum to overspin, $Q^2 + (J/M)^2 > M^2$, and therefore challenge the cosmic censorship conjecture [14] (see also Refs. [15–17] for comprehensive accounts and references therein). The correct angular momentum and energy range that these scalar

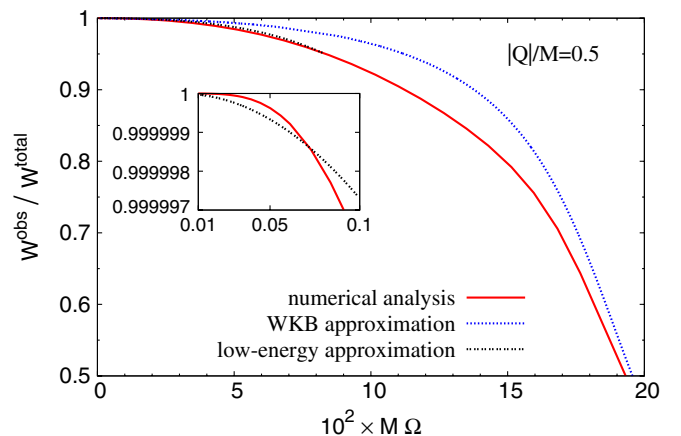


FIG. 9 (color online). The power observed at infinity is plotted as a function of Ω for $|Q|/M = 0.5$.

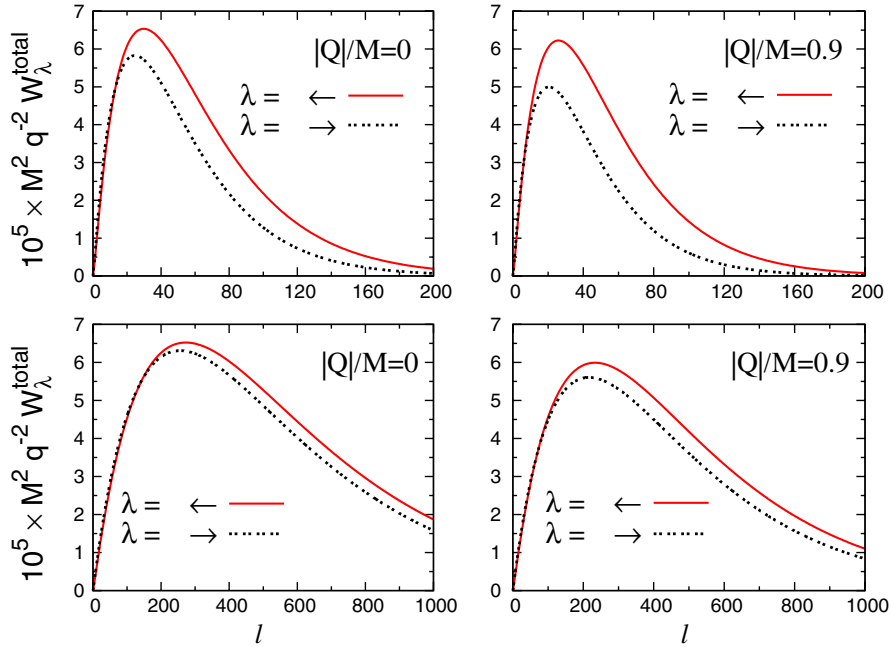


FIG. 10 (color online). The total power emitted as a function of l ($m = l$) is plotted. The two graphs above assume $\Omega = 0.99\Omega_{r_{\text{ph}}}$, and the two ones below assume $\Omega = 0.999\Omega_{r_{\text{ph}}}$, where $\Omega_{r_{\text{ph}}} \equiv (M/r_{\text{ph}}^3 - Q^2/r_{\text{ph}}^4)^{1/2}$. For $R_S \approx r_{\text{ph}}$ large l 's are excited.

particles must have depend on the black hole parameters. Because black holes with mass M , charge Q , and angular momentum J satisfy $M^2 \geq Q^2 + J^2/M^2$, the larger the mass M is the larger the angular momentum quantum number l of the ingoing particle must be. Accordingly, the particle energy range must be chosen in such a way that the inequality above is violated when the particle tunnels into the hole. A scalar particle with $l = 413$ and frequency in the range $\omega_0 \lesssim 4 \times 10^{-5}$ absorbed by a charged black hole with $M = 100$ and $|Q| = M - e$ would be in principle enough to overspin it [6]. In order to determine in what circular orbits our scalar source should lie in order to produce such low-energy particles we must

recall that $\omega_0 = m\Omega$. By choosing $m = l$ in order to maximize the emission rate, we obtain that the angular velocity of the source should satisfy $\Omega \lesssim 1/(10^7 M)$. Obviously, by choosing some other m , a different Ω range would be obtained accordingly. In Fig. 13, we plot the emission rate $\Gamma_{-\omega_0 l}$ of ingoing particles produced by such a source in the above Ω range. Whatever is the final verdict for this mechanism given by some complete quantum gravity calculation, this is remarkable that there is no *a priori* compelling reason to preclude the formation of naked singularities in the quantum realm. It is largely believed that *quantum gravity* should be able to unveil the physical structure of these “entities” making them nonsingular [18]

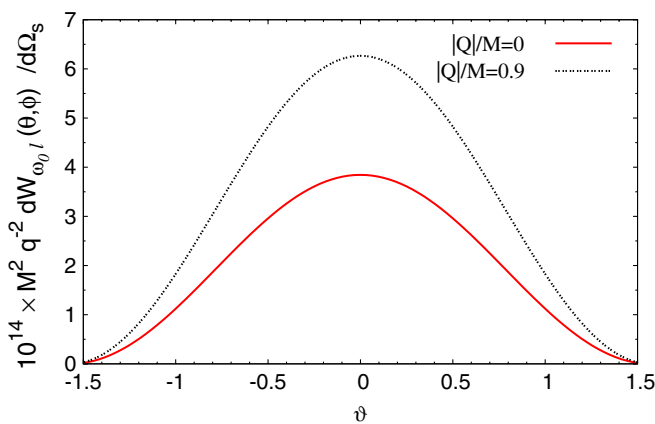


FIG. 11 (color online). The power angular distribution per unit of solid angle is plotted as a function of $\vartheta = \pi/2 - \theta$ for $\Omega = 0.001\Omega_{r_{\text{ph}}}$ and $l = m = 1$, where $\Omega_{r_{\text{ph}}} = (M/r_{\text{ph}}^3 - Q^2/r_{\text{ph}}^4)^{1/2}$.

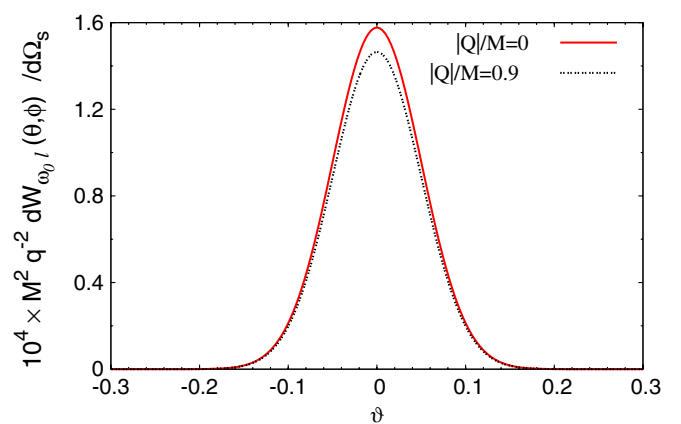


FIG. 12 (color online). The power angular distribution per unit of solid angle is plotted as a function of $\vartheta = \pi/2 - \theta$ for $\Omega = 0.999\Omega_{r_{\text{ph}}}$ and $l = m = 200$.

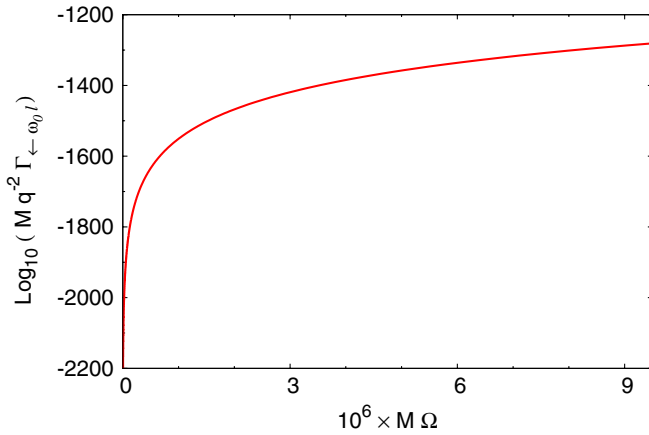


FIG. 13 (color online). The emission rate $\Gamma_{\omega_0 l}$ of particles with $l = 413$ and frequency in the range $0 < \omega_0 < 4 \times 10^{-5}$, which would overspin a black hole with $M = 100$ and $|Q| = M - e$ is plotted as a function of the source angular velocity Ω . We have chosen $m = l$ in order to maximize the emission rate.

and recovering the spacetime predictability. The generalized second law of thermodynamics could still be preserved if the initial entropy of the black hole were carried away by the degrees of freedom of some final debris assuming that naked singularities are unstable.

VI. FINAL REMARKS

We have considered the scalar radiation emitted from a monopole in circular geodesic orbits around a charged black hole. Emission rates and radiated powers were calculated using exact numerical and approximate analytical calculations, and shown to be in excellent agreement with each other in the proper regions. The net radiation which reaches asymptotic observers was also investigated and shown to decrease up to 50% when the source is close to the innermost geodesic circular orbit. The radiation angular distribution with respect to the orbit plane was also calculated and shown to be much sharper when the source is in relativistic motion. Eventually, a brief discussion about how the present particle production mechanism can be used to generate the ingoing modes considered in Refs. [6,7] was presented. The fermionic modes considered in Refs. [19,20] can be produced in a similar way.

ACKNOWLEDGMENTS

L. C. and G. M. are grateful to Conselho Nacional de Desenvolvimento Científico e Tecnológico (CNPq) for partial financial support. A. S. and G. M. would like also to acknowledge partial and full financial support from Fundação de Amparo à Pesquisa do Estado de São Paulo (FAPESP), respectively.

-
- [1] C. W. Misner, R. A. Breuer, D. R. Brill, P. L. Chrzanowski, H. G. Hughes, III, and C. M. Pereira, *Phys. Rev. Lett.* **28**, 998 (1972); R. A. Breuer, P. L. Chrzanowski, H. G. Hughes, III, and C. W. Misner, *Phys. Rev. D* **8**, 4309 (1973).
- [2] R. A. Breuer, *Gravitational Perturbation Theory and Synchrotron Radiation*, Lecture Notes in Physics (Springer-Verlag, Heidelberg, Germany, 1975).
- [3] E. Poisson, *Phys. Rev. D* **52**, 5719 (1995); L. M. Burko, *Phys. Rev. Lett.* **84**, 4529 (2000); V. Cardoso and J. P. S. Lemos, *Phys. Rev. D* **65**, 104033 (2002); J. Castiñeiras, L. C. B. Crispino, R. Murta, and G. E. A. Matsas, *Phys. Rev. D* **71**, 104013 (2005); L. C. B. Crispino, *Phys. Rev. D* **77**, 047503 (2008).
- [4] N. D. Birrel and P. C. W. Davies, *Quantum Fields in Curved Space* (Cambridge University Press, Cambridge, England, 1982).
- [5] S. A. Fulling, *Aspects of Quantum Field Theory in Curved Space-Time* (Cambridge University Press, Cambridge, England, 1989).
- [6] G. E. A. Matsas and A. R. R. da Silva, *Phys. Rev. Lett.* **99**, 181301 (2007).
- [7] S. Hod, *Phys. Rev. Lett.* **100**, 121101 (2008).
- [8] R. M. Wald, *General Relativity* (University of Chicago Press, Chicago, Illinois, 1984).
- [9] J. Castiñeiras and G. E. A. Matsas, *Phys. Rev. D* **62**, 064001 (2000).
- [10] C. Itzykson and J.-B. Zuber, *Quantum Field Theory* (McGraw-Hill, New York, New York, 1980).
- [11] I. S. Gradshteyn and I. M. Ryzhik, *Tables of Integrals, Series, and Products* (Academic Press, New York, New York, 1980).
- [12] E. Merzbacher, *Quantum Mechanics* (John Wiley, New York, New York, 1998).
- [13] L. C. B. Crispino, A. Higuchi, and G. E. A. Matsas, *Classical Quantum Gravity* **17**, 19 (2000).
- [14] R. Penrose, *Riv. Nuovo Cimento Soc. Ital. Fis.* **1**, 252 (1969).
- [15] C. J. S. Clarke, *Classical Quantum Gravity* **11**, 1375 (1994).
- [16] R. M. Wald, arXiv:gr-qc/9710068.
- [17] R. Penrose, *J. Astrophys. Astron.* **20**, 233 (1999).
- [18] A thought-provoking idea would be that naked singularities and elementary particles be low-energy-theory manifestations of some common quantum gravity structure, since all known elementary particles satisfy the constraint $M^2 < Q^2 + J^2/M^2$, where M , Q , and J should be associated here with the particle mass, electric charge, and spin, respectively. This would explain, e.g., why elementary neutral scalar particles have been never observed (since in this case $Q = J = 0$), and imply that the Higgs boson, if observed in the LHC/CERN, would be a composite rather than elementary scalar particle.
- [19] M. Richartz and A. Saa, *Phys. Rev. D* **78**, 081503(R) (2008).
- [20] S. Hod, *Phys. Lett. B* **668**, 346 (2008).